Journal of Alloys and Compounds 495 (2010) 532–536

Contents lists available at ScienceDirect

Journal of Alloys and Compounds

journal homepage: www.elsevier.com/locate/jallcom

Ionic exchange of Hf donor impurities in the wide-gap semiconductor Tm_2O_3

E.L. Muñoz [a], G.N. Darriba [a], A.G. Bibiloni [b], L.A. Errico [a,c], M. Rentería [a,*]

[a] Departamento de Física-IFLP (CONICET-UNLP), Facultad de Ciencias Exactas, Universidad Nacional de La Plata, C.C. 67, 1900 La Plata, Argentina
[b] Departamento de Física, Facultad de Ciencias Exactas, Universidad Nacional de La Plata, C.C. 67, 1900 La Plata, Argentina
[c] Universidad Nacional del Noroeste Bonaerense (UNNOBA), Monteagudo 2772, 2700 Pergamino, Buenos Aires, Argentina

ARTICLE INFO

Article history:
Received 23 July 2008
Received in revised form
11 September 2009
Accepted 6 October 2009
Available online 8 November 2009

Keywords:
Oxide materials
Mechanical alloying
Impurities in semiconductors
Hyperfine interactions
Ionic diffusion
Perturbed angular correlations (PAC)

ABSTRACT

The ionic exchange of Hf donor impurities in substitutional cationic sites of the cubic (*bixbyite*) phase of the wide-gap semiconductor Tm_2O_3 was studied. The doping process was performed by ball-milling-assisted solid-state reaction of Tm_2O_3 and neutron-activated *m*-HfO_2. ^{181}Ta atoms, obtained by the β-decay of the ^{181}Hf-isotope, were used as probes in time-differential perturbed-angular-correlation (TDPAC) experiments carried out after each step of the doping process. The measured hyperfine interactions at ^{181}Ta sites enabled the electric-field gradient (EFG) characterization at representative Hf impurity sites of each step of the process. The efficiency and substitutional character of the exchange process is discussed and elucidated in the framework of an empirical EFG systematic established in isostructural rare-earth *bixbyite* sesquioxides.

1. Introduction

Mechanical alloying, in combination with thermal treatments, is a versatile and non-expensive preparation method able to produce equilibrium as well as non-equilibrium materials. For this reason, the synthesis and development of materials by thermal-assisted mechanical alloying has been extensively studied.

In this kind of methods, high-energy mills are used, where the starting materials are repeatedly submitted to deformation, fracturing, and welding. In general, these processes induce the refinement of the microstructure up to the nanoscale, giving rise to inter-diffusion and mixing of the reacting elements. The way mixing occurs was the subject of different studies and models (see, e.g., Ref. [1] and references therein). In order to clarify the role played by each step of the mechanical alloying, it is necessary to obtain experimental information on the way the mixing and inter-diffusion proceed.

Thermal treatments also introduce structural and chemical local changes at the atomic sites. Local properties are also affected by global changes in the system such as variation in the interatomic distances, changes in the mean composition, etc. One way to investigate structural and electronic properties at the atomic scale are hyperfine techniques [2,3]. Nuclear methods and, in particular, the time-differential perturbed-angular correlations (TDPAC) spectroscopy have been extensively applied to study materials to elucidate the subnanoscopic scale environment(s) of impurities or constituent atoms of solids (see, e.g., Refs. [4,5]). In the case of TDPAC, a suitable probe isotope, generally an impurity in the system under study, is used and the information provided, at this probe site, is given as a product of a nuclear and an extra nuclear quantity. In the case of electric quadrupole interactions, the nuclear quantity is the nuclear quadrupole moment (Q), characteristic of a given nuclear state of spin I, which interacts with the electric-field gradient (EFG) at the nuclear position. Due to the r^{-3} dependence of the EFG operator from the charge sources, the EFG mostly originates in the non-spherical electronic charge density close to the impurity nucleus. For this reason, TDPAC technique can be used as a powerful tool in order to study the local and non-local changes induced by mechanical alloying and by thermally activated inter-diffusion mechanisms.

In this work we study the ball-milling-assisted solid-state reaction between neutron-activated *m*-HfO_2 and the oxide under study (the *bixbyite* Tm_2O_3) in order to follow the doping process of ^{181}Hf donor impurities in the semiconductor Tm_2O_3. For this study four samples were successively prepared. These samples were obtained at the end of each step of the doping process and the TDPAC technique was then used to characterize the samples to elucidate the effect of each variable (milling time, temperature, etc.) of the thermally-assisted solid-state reaction process. The obtained hyperfine parameters were compared to those of *m*-HfO_2 and

* Corresponding author. Tel.: +54 221 4246062; fax: +54 221 4252006.
E-mail address: renteria@fisica.unlp.edu.ar (M. Rentería).

0925-8388/$ – see front matter © 2009 Elsevier B.V. All rights reserved.
doi:10.1016/j.jallcom.2009.10.038

those expected for Tm_2O_3 using a well established EFG systematics for ^{181}Ta in *bixbyte* sesquioxides. As we will show, we can determine the effect played by the milling and the thermal treatments, showing the capability of the TDPAC technique to follow a doping process and to give information about the mixing and inter-diffusion processes. We also demonstrate the efficiency of the ball-milling-assisted solid-state reaction process to locate Hf donor impurities at cationic sites of the Tm_2O_3 semiconductor.

2. Experimental

2.1. The TDPAC technique: basic principles, experimental set-up and data reduction

The TDPAC technique (see, e.g., Ref. [2,3]) rests on the fact that, due to the conservation of angular momentum, the probability of emission of a photon in a definite direction in a nuclear decay is strictly correlated with the orientation of the nuclear spin. Then, in a radioactive source with the nuclei randomly oriented, it is possible to select a set of nuclei with a particular spin orientation detecting the first radiation γ_1 of a γ–γ cascade in a fixed direction $\vec{k}_1$. The detection of the second γ-ray, γ_2, will therefore show a certain angular distribution pattern with respect to the $\vec{k}_1$ direction. The density of probability $W(\theta, t)$ of finding the second emission in the direction $\vec{k}_2$, detected at an angle θ with respect to $\vec{k}_1$, will be perturbed if, during the time t the nucleus remains in the intermediate level, interaction with extra-nuclear fields occurs.

Thus, $W(\theta, t)$ is written as [3]:

$$W(\theta, t) = 1 + A_{22}G_{22}(t)P_2(\cos\, q), \tag{1}$$

A_{22} being the anisotropy of the cascade that only depends on nuclear properties and $P_2(\cos\theta)$ the second-order Legendre polynomial. Higher terms in Eq. (1) are negligible in the case of the ^{181}Ta cascade due to the small values of the A_{44} coefficients. In the absence of magnetic fields, the perturbation function $G_{22}(t)$ contains all the information of the hyperfine interaction between the nuclear-electric–quadrupole moment Q and the extra-nuclear EFG at each nucleus. This EFG is a consequence of the charge density distribution that depends on the atomic surrounding of the probe and on the nature of chemical bonds. For polycrystalline samples and a nuclear spin $I = 5/2$ of the intermediate nuclear level of the cascade, the perturbation factor $G_{22}(t)$ for static electric–quadrupole interactions has the form:

$$G_{22}(t) = \sum_i f_i \left\{ S_{20,i} + \sum_{n=1}^{3} [S_{2n,i} \cos(\omega_{n,i}t) e^{-\delta_i \omega_{n,i} t}] \right\} \tag{2}$$

where f_i is the relative fraction of nuclei that experiences a given perturbation. The ω_n interaction frequencies are related to the quadrupole frequency $\omega_Q = eQV_{ZZ}/40\hbar$ by $\omega_n = g_n\omega_Q$. The g_n and S_{2n} coefficients are known functions [6] of the asymmetry parameter $\eta = (V_{XX} - V_{YY})/V_{ZZ}$, where V_{ii} are the principal components of the EFG tensor that are arbitrarily labeled according to $|V_{XX}| < |V_{YY}| < |V_{ZZ}|$. The exponential functions in Eq. (2) account for a Lorentzian frequency distribution of relative width δ around ω_n.

In the experiments presented in this work, we made use of the well known 133–482 keV γ–γ cascade in ^{181}Ta, produced after the β^- nuclear-decay of the ^{181}Hf isotope. The experiments were performed using the PACAR spectrometer [7], constructed with a fast–fast coincidence logic and based on eight home-made fast-differential discriminators and four BaF_2 detectors in a coplanar 90° arrangement. The BaF_2 crystals were designed to improve the energy and time resolution of the detectors and to obtain high counting rates [7]. The time resolution of the spectrometer for ^{181}Ta γ-rays is 0.65 ns (FWHM).

Eight coincidence spectra, $C_{ij}(t)$, four taken between detectors positioned with 180° symmetry and four of eight possible with 90° symmetry, were simultaneously recorded in an 8 K-memory multichannel analyzer. For each t value, $C_{ij}(t)$ is the number of events in which the first γ-ray is detected by detector i and, after a time t, the second is detected by detector j. The coincidence spectra, corrected for accidental events, were combined to obtain:

$$W(180^\circ, t) = [C_{13}(t)C_{31}(t)]^{1/2}[C_{24}(t)C_{42}(t)]^{1/2} \tag{3}$$

and

$$W(90^\circ, t) = [C_{12}(t)C_{21}(t)]^{1/2}[C_{34}(t)C_{43}(t)]^{1/2} \tag{4}$$

Finally, the asymmetry ratio or spin–rotation curve $R(t)$ becomes:

$$R(t) = 2\frac{W(180^\circ, t) - W(90^\circ, t)}{W(180^\circ, t) + 2W(90^\circ, t)} \approx A_{22}^{\exp} G_{22}(t), \tag{5}$$

$A_{22}^{\exp}$ being the effective anisotropy of the cascade for a certain experimental condition.

Theoretical functions of the form $A_{22}{}^{\exp}G_{22}(t)$ (see Eq. (2)), folded with the time–resolution curve, were fitted to the experimental $R(t)$ spectra in order to extract the parameters f_i, $\omega_{Q,i}$, η_i, and δ_i of each hyperfine interaction.

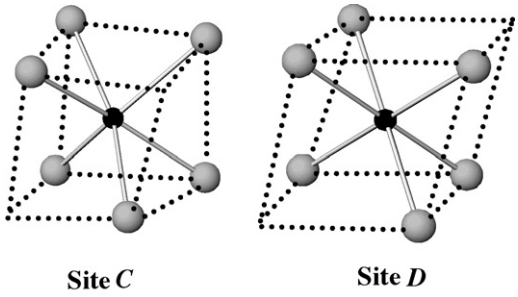

Fig. 1. Nearest-neighbor (NN) oxygen distribution around each cationic site (black atom) in the *bixbyite* structure.

2.2. Sample preparation and TDPAC measurements

Under suitable conditions, Fe, Mn, Sc, In, Tl, Y, and all the rare-earth elements form a sesquioxide. Polymorphism is common among the rare-earth oxides and below about 2300 K three polymorphous crystallographic structures have been found [8]: the hexagonal A-, the monoclinic B-, and the cubic C-form (*bixbyite*). In the cubic structure, the cations form a nearly cubic face-centered lattice (space group *Ia*3) in which six out of the eight tetrahedral sites are occupied by oxygen atoms. The elementary cell of the oxide lattice consists of eight such cubes, containing 32 cations and 48 oxygen ions. Two non-equivalent cationic sites, called *C* and *D*, both six-fold oxygen-coordinated, characterize the structure. Their relative abundance in the lattice is $(f_C/f_D) = 3$. Site *D* is axially symmetric and can be locally described as a cation surrounded by six oxygen atoms located at the corners of a distorted cube, leaving two corners of a diagonal free (D_{3d} point-group symmetry). At site *C* the cube is more distorted (C_2-symmetry) and the six oxygen atoms leave two corners on a face diagonal free (see Fig. 1).

In conclusion, according to the symmetry of both non-equivalent cationic sites of Tm_2O_3, one should expect that, if Hf homogenously substitutes Tm atoms in the *bixbyite* structure, two hyperfine interactions characterized by η_D close to 0 for the less intense interaction and a large η_C value for the other. Also, the frequency associated with site *D* should have twice the value of the frequency associated with the site *C*.

A ball-milling-assisted solid-state reaction, between neutron-activated *m*-HfO_2 and the oxide under study, was used in order to achieve the doping of ^{181}Hf atoms in the Tm_2O_3 semiconductor. The starting materials for this experiment were 5 mg of *m*-HfO_2 (Aldrich, 98% of metallic purity) and 800 mg of C-Tm_2O_3 (Alfa AESar, 99.99% of metallic purity). The *m*-HfO_2 powder was encapsulated in air at atmospheric pressure in a sealed quartz tube and irradiated with thermal neutrons (with a flux of 2×10^{13} neutrons $cm^{-2}\, s^{-1}$) in the RA-3 reactor of the National Atomic Energy Commission (CNEA, Argentina) in order to obtain the required ^{181}Hf activity by means of the nuclear reaction ^{180}Hf(n,γ)^{181}Hf. The amount of initial powders was chosen to obtain a concentration of Hf impurities relative to Tm atoms of 1 at.%. The activated *m*-HfO_2 was manually mixed with the Tm_2O_3 powder and treated in air for 30 m at 1123 K and 60 m at 1273 K ("Sample I"). At the end of this thermal treatment the sample was charged into a cylindrical agate vial (10 cm^3 volume) with one agate ball (1.2 cm diameter) under air atmosphere; the ball-to-powder weight ratio was $R_{BP} = 3$. The ball milling was performed in a horizontal oscillatory mill (Restch MM2) with an operating cycle of 3 h. The frequency of the milling was 40(2) Hz ("Sample II"). Afterwards, 400 mg of Sample II was treated in air at atmospheric pressure for 16 h at 1273 K, 6.5 h at 1473 K, and 8 h at 1523 K ("Sample III"). The other half of Sample II was milled (one agate ball of 1.2 cm diameter was used, $R_{BP} = 6$) at 40(2) Hz for another 3 h. Then, this powder underwent the same thermal treatment as Sample III ("Sample IV"). In Table 1 (first two columns) we resume the preparation treatment of each sample. TDPAC measurements at RT in air were carried out on Samples I–IV immediately after their preparation.

3. Results and discussion

Fig. 2 shows the $R(t)$ spectra, and their corresponding Fourier transforms, taken at RT in air on the Tm_2O_3 sample series. Solid lines in the $R(t)$ spectra are the best least-squares fits of Eq. (5) to the experimental data. Solid lines in the Fourier spectra come from the Fourier transform of the $R(t)$ fits. Three hyperfine interactions were necessary to describe the $R(t)$ spectra of Fig. 2: Hfi 1, Hfi 2, and Hfi 3, their parameters being displayed in Table 1. In Sample I (manually mixed powders followed by a thermal treatment) only Hfi 1 was found [Fig. 2(a)]. As it was expected, their hyperfine parameters correspond to that of pure *m*-HfO_2 [7,9]. In this initial sample, the effect of the thermal treatment is not enough to start the Hf dif-

Table 1
Hyperfine parameters of the interactions found at RT after each step of the ^{181}Hf-doping process of the Tm_2O_3 samples (see Section 2.2). f_i and δ_i are expressed in % and ω_{Qi} in Mrad/s. When no errors are quoted it means that the parameter was kept fixed to enable the calculation of the other errors.

Sample	Preparation treatment	Hfi 1				Hfi 2				Hfi 3			
		f_1	ω_{Q1}	η_1	δ_1	f_2	ω_{Q2}	η_2	δ_2	f_3	ω_{Q3}	η_3	δ_3
Sample I	Manually mixed powders treated in air at 1123 K (0.5 h) + 1273 K (1 h)	100	125.6(5)	0.354(4)	4(3)								
Sample II	Sample I ball-milled 3 h at 40 Hz	91(1)	125.2(5)	0.364(5)	7.5(3)	6(1)	117.7(2)	0.76(1)	1.1(9)	3(1)	245.7(9)	0.18(2)	0.0(5)
Sample III	Sample II annealed in air 16 h at 1273 K + 6.5 h at 1473 K + 8 h at 1523 K	41(6)	125(1)	0.39(2)	8.0(8)	28(6)	115(1)	0	10(2)	31(5)	206(2)	0.0(1)	8(1)
Sample IV	Sample II milled 3 h at 40 Hz + Sample III's thermal annealing	39(6)	118(2)	0.1(1)	9(1)	40(5)	118.1(8)	0.49(1)	3.4(7)	21(5)	202(1)	0	3(1)

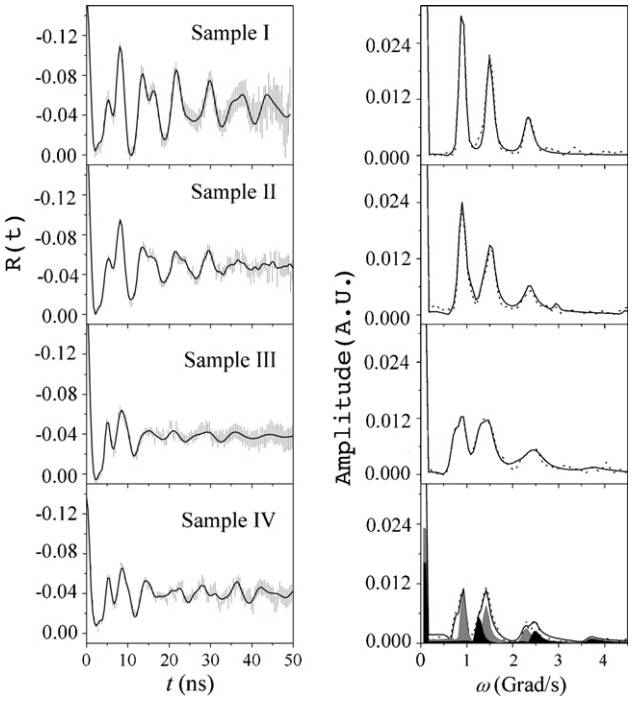

Fig. 2. $R(t)$ spectra (left) and their corresponding Fourier transforms (right) of (^{181}Hf $\rightarrow$)^{181}Ta in the Tm_2O_3 sample series (see Section 2.2 and Table 1) taken at RT in air. The frequencies ω_n associated with the hyperfine interactions Hfi 2 and Hfi 3 are shaded in grey and black, respectively, in the fourth Fourier spectrum. Note the change in scale of this spectrum.

fusion into the Tm-oxide lattice. But, after 3 h of ball milling, some changes occur. In effect, the Fourier spectrum of Sample II [Fig. 2(b)] consists basically on the peaks associated with pure *m*-HfO_2 but, in addition, a broadening of these peaks can be observed. Three interactions were necessary in order to reproduce the experimental $R(t)$ spectrum. The first interaction, which accounts for more than 90% of the pattern, is very similar to that obtained for pure *m*-HfO_2, but the increment of its distribution (see Table 1) indicates the presence of some degree of disorder in the local environment of the probes still located at cationic sites in *m*-HfO_2. In the case of the other two interactions, the more populated one (Hfi 2) is characterized by a high η value. On the other hand, Hfi 3 presents η close to 0, and the frequency associated with this interaction is twice as large as the asymmetric one (see Table 1). Based on the previous discussion, we associate these two interactions with the crystalline non-equivalent cation sites *C* and *D* of Tm_2O_3, respectively. In the case of Sample III [Fig. 2(c)], the spectra change drastically. In effect, the interaction previously associated with *m*-HfO_2 (Hfi 1) reduces its population from 90% to 41%. In addition, the η value departs a little from that of crystalline *m*-HfO_2 (see Table 1). The interactions Hfi 2 and Hfi 3 increase their populations up to 59%, showing that both the ball milling and the thermal treatment are necessary to obtain a high degree of ^{181}Hf substitution in the Tm_2O_3 lattice by Hf diffusion, once the *m*-HfO_2 structure is destabilized (as in Sample II). Nevertheless, the EFG distributions obtained for Hfi 2 and Hfi 3 are still rather high (8–10%). In Sample IV, the longer elapsed time of the milling process as well as the greater ball-to-powder weight ratio compared to those used in Sample III, followed by the same annealing treatment, originate interesting changes: although the amount of remanent HfO_2 remains the same (since it is proportional to the fraction of ^{181}Hf probes in Hfi 1, which remains at 40%, see Table 1), it is clear that the cation neighborhood in *m*-HfO_2 is distorted as shown by the strong change in the hyperfine parameters of Hfi 1; the population ratio $f_{\text{Hfi 2}}/f_{\text{Hfi 3}}$ increases up to

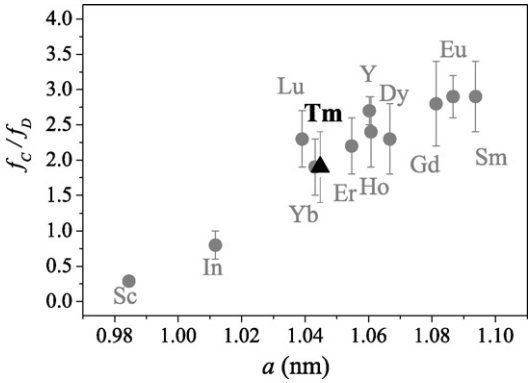

Fig. 3. Experimental ratio f_C/f_D as a function of the lattice parameter a for ^{181}Ta in cubic bixbyite sesquioxides (data taken from Refs. [10–15]). The black triangle corresponds to Tm_2O_3.

2:1 (in agreement with the ^{181}Ta systematics in *bixbyites* shown in Fig. 3) and the EFG distributions of Hfi 2 and Hfi 3 strongly diminish. In Fig. 2(d), the shaded peaks associated with the interaction frequencies of Hfi 2 and Hfi 3 reflect the low distribution of these interactions. Additionally, it can be seen that the dampening of the spectrum comes from the high distribution of Hfi 1 and also from the "destructive interference" originated on the superposition of the interaction frequencies of Hfi 2 and Hfi 3. To conclude, the hyperfine parameters ω_Q and η of Hfi 2 and Hfi 3 now agrees perfectly with the ^{181}Ta EFG systematics [10] shown in Fig. 4. It is important to mention that all the other points in this figure correspond to implanted samples. The excellent agreement of ω_Q and η at both cation sites of this oxide with the rest of the systematics shows the capability of the mechanochemical solid-state reaction process between the sesquioxide and neutron-activated *m*-HfO_2 to locate the probes at cation sites of the sesquioxide. From the Hfi 1 parameters in Sample IV one can deduce that the longer milling time produced a larger distortion of the *m*-HfO_2 structure or a further reduction of the grain size, which in any case seems to favor a more homogenous and better Hf exchange in the semiconductor matrix.

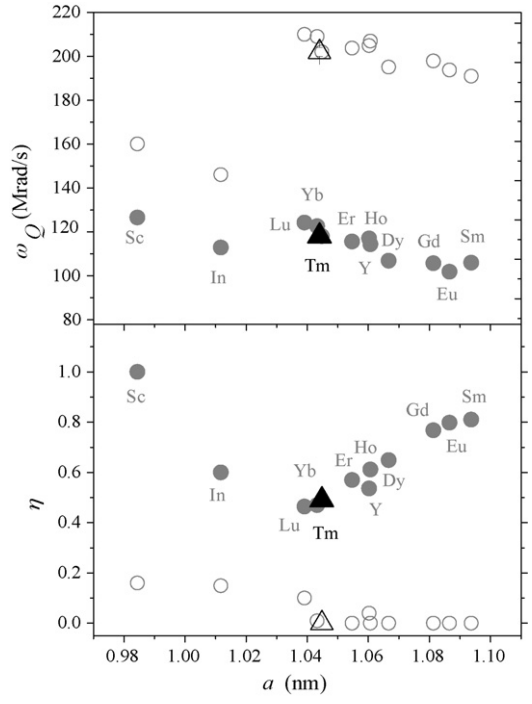

Fig. 4. Experimental quadrupole frequency and asymmetry parameter η for substitutional ^{181}Ta impurities at sites C (filled circles) and D (hollow circles) in bixbyites plotted as a function of the lattice parameter a (data taken from Refs. [10–15]). Back and hollow triangles correspond to results at sites *C* and *D* in Tm_2O_3, respectively. The errors are smaller than the symbols.

Finally, we want to comment previous results obtained applying the same doping method to Ho_2O_3. Ho_2O_3 presents the same crystalline structure that Tm_2O_3, but it is characterized by a lattice parameter *a* slightly larger (*a* = 10.606 Å) than that corresponding to Tm_2O_3 (*a* = 10.448 Å). In the case of Ho_2O_3, a milling time of 3 h was enough to achieve a high degree of Hf substitution at free-of-defect cationic sites of Ho_2O_3. This result shows that the lattice parameter may play an important role in the doping process.

4. Conclusions

In this work, the TDPAC technique was applied to study the ionic exchange of Hf donor impurities at substitutional cation sites of the semiconductor Tm_2O_3. The doping process was performed through a ball-milling-assisted solid-state reaction of neutron-activated *m*-HfO_2 and Tm_2O_3. The hyperfine parameters found in this work for ^{181}Ta probes located at both cation sites of Tm_2O_3 and those predicted by the ^{181}Ta EFG systematics established in rare-earth *bixbyites* doped by ion-implantation of ^{181}Hf($\rightarrow^{181}$Ta) ions agree excellently. This agreement shows the capability of this solid-state reaction method to locate the impurities at cation sites of the sesquioxide. In addition, the highly localized information obtained in the TDPAC experiments enable us to follow and quantify (through the Hfi fractions) the efficiency of the doping process after each step of the ionic exchange method. Our results show that high temperature treatments, performed after the milling, are necessary to achieve a high degree of Hf substitution in the cation sublattice of the Tm_2O_3 structure. In the same way, results obtained for Ho_2O_3 suggest that the milling time necessary to obtain a high degree of Hf substitution may depend, among other characteristics of these impurity-oxide systems, on the available size at the cationic sites. We can conclude that shorter milling times would be expected for a high substitution of Hf in oxides with larger lattice parameters.

Acknowledgements

This work was partially supported by Agencia Nacional de Promoción Científica y Tecnológica (ANPCyT) under PICT98 03-03727, Consejo Nacional de Investigaciones Científicas y Técnicas (CONICET) under PIP6032 and PIP0002, and Fundación Antorchas, Argentina, and the Third World Academy of Sciences (TWAS), Italy, RGA 97-057. A.G.B., L.A.E., and M.R. are members of CONICET, Argentina.

References

[1] A.F. Cabrera, F.H. Sánchez, Phys. Rev. B 65 (2002) 094202.
[2] A. Lerf, T. Butz, Hyperfine Interact. 36 (1987) 275.
[3] H. Frauenfelder, R. Steffen, in: K. Siegbahn (Ed.), α-, β-, and γ-Ray Spectroscopy, vol. 2, North-Holland, Amsterdam, 1968, p. 917;
G. Schatz, A. Weidinger, Nuclear Methods and Applications (translated by J.A. Gardner), John Wiley & Sons, Chichester, 1996, p. 63.
[4] A. Lerf, T. Butz, Angew. Chem. Int. Ed. Engl. 26 (1987) 110;
T. Klas, J. Voigt, W. Keppner, R. Wesche, G. Schatz, Phys. Rev. Lett. 57 (1986) 1068;
R. Vianden, U. Feuser, Phys. Rev. Lett. 61 (1988) 1981;
N. Achtziger, W. Witthuhn, Phys. Rev. B 47 (1993) 6990;
D. Lupascu, M. Uhrmacher, K.P. Lieb, J. Phys.: Condens. Matter 6 (1994) 10445;
S. Lany, P. Blaha, J. Hamann, V. Ostheimer, H. Wolf, T. Wichert, Phys. Rev. B 62 (2000) R2259;
J. Meersschaut, C. L'abbe, M. Rots, S.D. Bader, Phys. Rev. Lett. 87 (2001) 107201;
J.M. Ramallo López, M. Rentería, E.E. Miró, F.G. Requejo, A. Traverse, Phys. Rev. Lett. 91 (2003) 108304;
M. Forker, S. Muller, P. de la Presa, A.F. Pasquevich, Phys. Rev. B 68 (2003) 14409.

[5] L.A. Errico, G. Fabricius, M. Rentería, P. de la Presa, M. Forker, Phys. Rev. Lett. 89 (2002) 55503;
L.A. Errico, G. Fabricius, M. Rentería, Phys. Rev. B 67 (2003) 144104, and references therein.
[6] L.A Mendoza-Zélis, A.G. Bibiloni, M.C. Caracoche, A.R. López-García, J.A. Martínez, R.C. Mercader, A.F. Pasquevich, Hyperfine Interact. 3 (1977) 315.
[7] M. Rentería, A.G. Bibiloni, G.N. Darriba, L.A. Errico, E.L. Muñoz, D. Richard, J. Runco, Hyperfine Interact 181 (2008) 665.
[8] L. Eyring, in: K.A. Gschneidner, L. Eyring (Eds.), Handbook on the Physics and Chemistry of Rare Earths, North-Holland, Amsterdam, 1979, p. 337.
[9] A. Ayala, R. Alonso, A. López-García, Phys. Rev. B 50 (1994) 3547.
[10] L.A. Errico, M. Rentería, A.G. Bibiloni, K. Freitag, Physica B 389 (2007) 124.
[11] M. Rentería, F.G. Requejo, A.G. Bibiloni, A.F. Pasquevich, J. Shitu, K. Freitag, Phys. Rev. B 55 (1997) 14200.
[12] A.F. Pasquevich, A.G. Bibiloni, C.P. Massolo, M. Rentería, J.A. Vercesi, K. Freitag, Phys. Rev. B 49 (1994) 14331.
[13] M. Rentería, A.G. Bibiloni, F.G. Requejo, A.F. Pasquevich, J. Shitu, L.A. Errico, K. Freitag, Mod. Phys. Lett. B 12 (1998) 819.
[14] M. Rentería, K. Freitag, L.A. Errico, Hyperfine Interact. 120/121 (1999) 449.
[15] L.A. Errico, M. Rentería, A.F. Pasquevich, A.G. Bibiloni, K. Freitag, Eur. Phys. J. B 22 (2001) 149.